Theoretical study of the expansion of supercritical water in a capillary device at the output of a hydrothermal oxidation process

Frederic Marias, Stéphanie Vielcazals, Pierre Cézac, Jacques Mercadier, François Cansell

Theoretical study of the expansion of supercritical water in a capillary device at the output of a hydrothermal oxidation process

F. Marias [a,*], S. Vielcazals [a], P.Cezac [a], J. Mercadier [a], F. Cansell [b]

[a] *Laboratoire de Thermique Energétique et Procédés (LaTEP), Ecole Nationale Supérieure d'Ingénieurs en Génie des Technologies Industrielles, Université de Pau et des Pays de l'Adour, EA 1932, Rue Jules Ferry, B.P. 7511, 64075 Pau Cedex, France*

[b] *Institut de Chimie de la Matière Condensée de Bordeaux (ICMCB), CNRS-UPR 9048, Université Bordeaux 1, 87 Avenue Dr. Schweitzer, 33608 Pessac Cedex, France*

Abstract

This paper deals with the expansion of supercritical water at the output of the reactor of a supercritical water oxidation process. Inside such reactors, a common value of the working pressure is approximately 25 MPa. The fluid exhausting the reactor mainly contains water and carbon dioxide and salts. The operating pressure needs to be dropped in order to separate the different constituent of the fluid and to send back to environment the clean effluents. The behaviour of the salts held within the supercritical water is very specific. Indeed, at high pressure, the salts are present at the solid state, but once some liquid water appears, a part of the salts is dissolved into this liquid. Thus, in order to be separated by classical gas/solid separation at moderate pressure, the process stream needs to be carefully expanded. This paper presents a mathematical model that has been build in order to design a capillary device for this expansion. The governing equations of the model are presented as well as the way it has been solved. Some computations around a nominal operating conditions point are performed. These computations have led us to the design of an experimental device.

Keywords: Supercritical water oxidation; Modelling; Expansion; Salts; Thermodynamic approach

1. Introduction

Organic wastes produced by our societies need to undergo some treatment in order to be destroyed (at least to become inert for the environment) and to recover the potential energy that their constitutive molecules hold. The transformation of these organic species requires the addition of an oxidant in order to transform their carbon into carbon dioxide and their hydrogen into water. To complete this transformation within a short time, the use of activators of reaction is very frequent. Indeed, in the case of biological treatment, the activator is bacteria media, while it is temperature in the case of incineration, pyrolysis or gasification. Hydrothermal oxidation uses both temperature and pressure as activators. The main effect of pressure is to homogenise the reactive media and to enhance transfer inside this homogeneous phase (at high pressure, oxygen can be completely dissolved into water holding organic wastes) while the effect of temperature is to enhance the chemical reaction rate.

One of the main advantages of hydrothermal oxidation is that this mode of operation is compatible with sustainable development. The by products of this process are nontoxic. Carbon and hydrogen are respectively converted into carbon dioxide and water while hetero-atoms (N, Cl, S, ...) lead to atmospheric nitrogen and mineral acids [1–4]. Among the different process of hydrothermal oxidation, supercritical water oxidation is the most efficient because it operates at high pressure (25 MPa) but also at higher temperature (above the critical point of pure water 647 K) than other hydrothermal oxidation processes (di-phasic wet oxidation and under critical homogenous oxidation) leading to higher chemical reaction rates, and thus to shorter reactors [5]. It is also very interesting from the environmental point of view because the mineral acids that can be present in the waste itself (NaCl, Na_2SO_4, $(NH_4)_3PO_4$, ...), or that can be produced inside the reactor itself (HCl, H_2SO_4, ...) [6] are at the solid state

* Corresponding author. Tel.: +33 559 407 809.
E-mail address: Frederic.marias@univ-pau.fr (F. Marias).

Nomenclature

b	empirical parameter ($kg^{1/2}\,mol^{-1/2}$)
C	molar concentration of salts inside the capillary ($mol\,l^{-1}$)
d	inner diameter of the capillary (m)
e^{esu}	electronic charge in esu (4.8029×10^{-10} esu).
ΔG_i°	standard molal Gibbs free energy of formation ($J\,mol^{-1}$)
ΔG_R°	standard Gibbs free energy of reaction ($J\,mol^{-1}$)
h	specific enthalpy of the reactive media ($J\,kg^{-1}$)
H	heat transfer coefficient with the surroundings ($W\,m^{-2}\,K^{-1}$)
ΔH_{NaCl}^F	latent heat of fusion of NaCl ($J\,mol^{-1}$)
I	ionic strength
k_B^{erg}	Boltzmann constant in erg (1.38045×10^{-16} erg)
K	equilibrium constant
L	total length of the capillary (m)
L_{sat}	length of occurrence of liquid phase (saturation) (m)
%Liq	percentage of the incoming salt in the liquid phase at the capillary output
$\dot{m}$	mass flow rate of mixture inside the capillary ($kg\,h^{-1}$)
m_i	molality of species i ($mol\,kg^{-1}$)
N^0	Avogadro number (mol^{-1})
P	pressure inside the capillary (Pa)
P_{atm}	atmospheric pressure (Pa)
P_{sat}	pressure of saturation of pure water at a given temperature (Pa)
R	gas constant ($J\,mol^{-1}\,K^{-1}$)
%Sol	percentage of the incoming salt in the solid phase at the capillary output
T	temperature inside the capillary (K)
T_{NaCl}^F	temperature of fusion of NaCl (K)
u	local velocity of the mixture ($m\,s^{-1}$)
Δu	cohesive energy ($J\,mol^{-1}$)
v	molar volume ($m^3\,mol^{-1}$)
%Vap	percentage of the incoming salt in the vapour phase at the capillary output
y_{NaCl}	solubility of NaCl in the vapour phase

Greek symbols

α_{NaCl}^v	parameter
β_{NaCl}^v	parameter
γ	activity coefficient
$\gamma^\pm$	mean activity coefficient
δ	solubility parameter $(J\,m^{-3})^{1/2}$
ε	pair potential energy parameter (J)
μ	dynamic viscosity of the reactive media (Pa s)
$\Delta\xi/\Delta x$	lineic pressure drop ($Pa\,m^{-1}$)
ν_i	stoichiometric coefficient of the ith species
ρ	density of the reactive media ($kg\,m^{-3}$)
τ_{xj}	stress tensor in direction x linked to velocity gradient in direction j
ψ	dielectric constant of water

Subscripts

in	inlet of the capillary tube
out	outlet of the capillary tube

above the critical point of pure water because of the low value of its dielectric constant [7]. At present time a lot of research is performed on the particular topic of salts behaviour into supercritical water both on the modelling and on the experimental point of view [8–12].

This solid state makes the separation between the process stream and the salts easier. Indeed if this separation is performed while mineral acids are kept at solid state, there is no need to use a waster water treatment that would be necessary to recover minerals dissolved in water. Such a supercritical fluid solid separation can be handled into a cyclone and this is what we plan to do. However, in order to limit the cost of such a device, it is necessary to lower both the pressure and the temperature of the fluid to process. Our proposal is to use a capillary device in order to expand the fluid and thus to reduce its pressure and consequently its temperature. The alternative to use such a device is motivated by the fact that regulation systems that are able to control a pressure drop of 250 bar are very complex to handle when the flow is loaded with solid particles.

The first part of this article gives insights into the device we actually study. The specifications (in terms of operating conditions of the incoming fluid) and the geometrical parameters to design are given in this part. Then, in a second part, the mathematical model that has been used to compute this data is presented. This model is divided into two parts. The first one deal with the expansion itself while the second part deals with thermodynamical aspects that allow for the prediction of the distribution of salts between the supercritical, the vapour and the liquid phase that might occur during the expansion of the process stream. Finally, some results of the model are presented. As a preliminary, the influence of the diameter of the capillary on its length is discussed. Then, the next set of results focuses on the expansion at nominal conditions. Evolution, of temperature, pressure as well as distribution of minerals between the phases is presented versus the length of the capillary device. Finally, the influence of the operating conditions on the length of the capillary and on the possible recover of salts at solid state is discussed.

2. Device under study

The device under study is depicted in Fig. 1. It is composed of a storage tank where mineral acids can are dissolved into pure water. This mixture is fed to a heater by a high pressure pump at 25 MPa. The control loop for the mass flow rate of mixture entering the process is not represented on the figure. The fluid

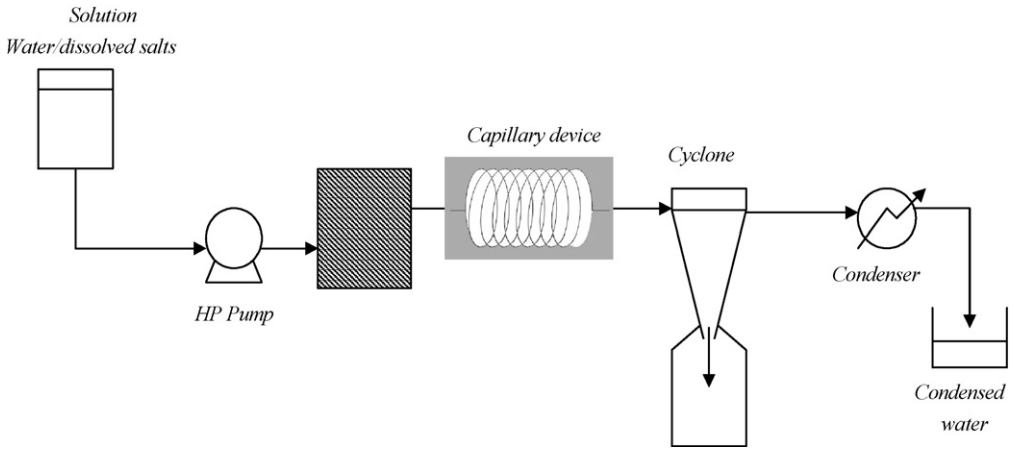

Fig. 1. Presentation of the device under study.

then enters the heater that allows for the control of the temperature of the stream entering the capillary tube. Basically, this heater represents the reactor of the supercritical water oxidation process that would lead to energy release and thus heating up of the process stream. The mixture is then expanded into the capillary device under study before entering the cyclone. The capillary is insulated by a calcite shell. Inside the cyclone the solid/gas separation is performed under the effect of centrifugal force acting at high speed of rotation. The free of solids vapour exhausting the cyclone is then condensed and collected into a tank. The capillary that needs to be designed have to be able to expand the following process stream:

- inlet mass flow rate: $\dot{m}_{\text{in}} = 20\,\text{kg}\,\text{h}^{-1}$;
- inlet pressure: $P_{\text{in}} = 25\,\text{MPa}$;
- inlet temperature: $T_{\text{in}} = 873\,\text{K}$;
- inlet salts concentration: $C_{\text{in}} = 0.5\,\text{mol}\,\text{l}^{-1}$;

As it has been quoted into the introduction, and, as it is explained in the literatures [13–15], the process stream entering the cyclone must have a pressure of the order of magnitude of the atmospheric pressure. The role of the capillary device is to expanded the fluid under the combined effect of:

- Linear pressure drop inside the tube.
- Decrease of the density of the mixture (under both pressure and temperature effects).
- Increase in the velocity of the fluid (by conservation of the total mass flow rate of mixture) which, in turns, increases the linear pressure drop.
- Decrease of the temperature of the fluid (by conservation of the total energy of the fluid) which, in turns, decreases the density of the fluid.

In order to compute the length of the capillary device, we impose the value of the pressure at the outlet of the tube to be equal to atmospheric pressure:

$$P_{\text{out}} = P_{\text{atm}} = 0.1\,\text{MPa} \tag{1}$$

3. Mathematical modelling

In this section, the governing equations responsible for the expansion of the fluid are presented. We first give insights on the assumptions that have been formulated in order to translate the physical and chemical phenomena into mathematical formalism.

3.1. Assumptions

Inside the capillary, the mixture is composed of water and salts. Thus, the prediction of the thermodynamical properties of the mixture (enthalpy and density) should take into account the influence of these salts as well as the influence of temperature and pressure.

However, because of the low concentration of salts inside the mixture, the main part of the total mass flow rate of the fluid flowing inside the reactor is water. This is the reason why we assume that the process stream is pure water. These properties are computed from the IAPWS formulation for pure water [16]. So the first assumption is:

Assumption 1. Thermodynamical properties (specific enthalpy and density) of the reacting media are assumed to be equal to pure water properties.

The second assumption (which is closed to the first one) is relative to the transport properties of the mixture. Indeed, with the same justification than Assumption 1, we postulate:

Assumption 2. Transport properties (thermal conductivity and viscosity) of the reacting media are equal to pure water properties and are computed from the IAPWS formulation for pure water.

Given some general operating conditions (temperature at inlet is above 450 °C and pressure is 25 MPa) and a mass flow rate of $20\,\text{kg}\,\text{h}^{-1}$, the Reynolds's number at the entrance of the capillary can be evaluated: $Re = 58\,000$. Thus the flow field inside the tube is fully turbulent. That is why we assume the plug flow mode of operation of this capillary. Thus, in stationary mode of operation, the state variables of the system are one-dimensional. This leads to the third assumption:

Assumption 3. In stationary mode of operation, the system under study is considered as one-dimensional.

Although the whole apparatus is thermally insulated, it is obvious that thermal losses exist. They have to be taken into account into the energy balance of the device. To compute these losses, we have assumed that at each location of the reactor, a specific heat flux was lost according to Newton's law for heat transfer.

Assumption 4. The specific heat flux by the thermal losses is expressed as:

$$\varphi_{\text{lost}} = H(T - T_{\text{ext}}) \tag{2}$$

In this expression, H represents the overall heat transfer coefficient with the surroundings, T and T_{ext} stand, respectively for the local temperature of the fluid and the external temperature.

As it has been quoted into the introduction, a lot of mineral acids can be present within the fluid to process. A rigorous study should take into account the specificity of each of these salts. However, in order to simplify the mathematical treatment and to simplify the thermodynamical description of the system we suppose the salts to be composed solely of NaCl.

Assumption 5. The salts are supposed to be solely composed of NaCl.

When the pressure and temperature are lowered, we might reach the saturation point during the expansion. This means that water will exist under different phases. The salts present in the mixture have different affinities for each of these phases. In order to compute the distribution of the salts between these phases, we assume that the thermodynamical equilibrium of the salts is reached. This means that we do not take into account the time that would be required to dissolve salts from solid state to liquid for example. This is a way to maximise the estimation of the salts dissolved within the liquid phase when saturation is reached. This leads to the final assumption.

Assumption 6. The distribution of salts between the different phases of water is computed assuming thermodynamical equilibrium to be reached at each location of the capillary.

3.2. Governing equations

One of the aims of a mathematical model is to provide some information about the physical and chemical phenomena that can occur in an apparatus when either this apparatus does not exist or some data are inaccessible to physical measurement. For example, in our case, we expect the model to be able to describe the evolution of the salt concentration as well as the temperature along the capillary. In order to obtain such information, we need to write some mathematical equations that translate physical and chemical phenomena into mathematical formalism. Basically, these equations postulate that in stationary mode of operation, mass, species, momentum and energy are conserved over a control volume of our choice. Moreover, in order to compute the distribution of the salts between the different phases, we assume that at each location of the capillary, the Gibb's free energy has reached her minimal value.

In the following paragraph we show the governing equations in their "derivative" form inside each of the three reactors.

3.2.1. Total mass conservation

$$\frac{\partial \rho u}{\partial x} = 0 \tag{3}$$

where ρ stands for the local density of the mixture and u for its velocity. This equation states that within the reactor mass is neither created nor disappeared.

3.2.2. Momentum conservation

As it has been quoted into Assumption 3, we consider the system as one-dimensional. However, a complete formulation of the momentuum equation should include a two-dimensional formulation of this equation because of the shear stress at the wall of the reactor. Indeed, this shear stress resutls in high radial gradients a this loccation. Thus the momentum balance is written as follows:

$$\frac{\partial \rho u u}{\partial x} = -\frac{\partial P}{\partial x} + \frac{\partial \tau_{xj}}{\partial x_j} \tag{4}$$

where P stands for the local pressure of the reacting media, and τ_{xj} for the stress tensor, in direction x, linked to a gradient of velocity in the direction j.

Moreover, in turbulent mode of operation, the stress tensor should include the Reynolds's stress tensor and an appropriate model to compute it. This would drastically complicate the mathematical description of the process. Thus, the choice that has been made here is to compute the divergence of the stress tensor as the local pressure drop over the control volume under consideration [17]. This computation has been done according to Churchill's correlation, valid for any Reynolds's number [18]. The resulting balance equation is then:

$$\frac{\partial \rho u u}{\partial x} = -\frac{\partial P}{\partial x} - \frac{\Delta \xi}{\Delta x} \tag{5}$$

where $\Delta\xi/\Delta x$ represents the local lineic pressure drop inside the capillary tube. This is a positive data of our model.

3.2.3. Energy conservation

Following the formalism used to derive the divergence of the stress tensor, one is able to compute the disspation (both viscous and turbulent) as [19]:

$$\Theta = u\frac{\Delta \xi}{\Delta x} \tag{6}$$

Then the balance of energy over the control volume is expressed as:

$$\frac{\partial \rho u h}{\partial x} = u\frac{\Delta \xi}{\Delta x} + u\frac{\partial P}{\partial x} + \frac{\partial}{\partial x}\left(\lambda \frac{\partial T}{\partial x}\right) - \frac{4H}{d}(T - T_{\text{ext}}) \tag{7}$$

where λ stands for the thermal conductivity of pure water and is computed according to Wagner and Kruse [16]. This equation states that the enthalpy of the fluid along the device is

- Increased by the dissipation of mecanical energy by friction (the term $\Delta\xi/\Delta x$ is positive).
- Decreased by the expansion (the term $\partial P/\partial x$ is negative).
- Decreased by conduction and by external losses (the term $\partial T/\partial x$ is negative).

3.2.4. Vapour fraction

The vapour fraction needs to be computed when saturation has been reached. If both temperature and pressure are above the critical point of pure water, or, if the operating pressure is lower than the saturation pressure we postulate:

$$\omega = 1 \tag{8}$$

If the saturation curve has been reached, then the vapour fraction is computed replacing Eq. (8) by the following:

$$P = P_{\text{sat}}(T) \tag{9}$$

This leads to an ordinary differential and algebraic system of seven unknowns (u, P, T, ρ, h, μ, ω) with seven Eqs. (3), (5), (7), (9)–(12).

3.2.5. Models for density, enthalpy to weight and viscosity

Finally, to close the problem, one needs to write equations for the computation of density and the computation of enthalpy. These equations are issued from the IAPWS formulation for pure water Eq. (8) (see Assumption 1) and they are written as:

$$\rho = \rho_{\text{m}}(P, T, \omega) \tag{10}$$

$$h = h_{\text{m}}(P, T, \omega) \tag{11}$$

$$\mu = \mu_{\text{m}}(P, T, \omega) \tag{12}$$

3.2.6. Salts accountability

As long as the rate of vapourization is equal to 1, salt is supposed to be distributed between a vapour phase and a solid phase. The model of Shin et al. [20] was used to predict the solubility, in terms of mass fraction of salt in the vapour phase (y_{NaCl}):

$$\ln(y_{\text{NaCl}}) = \frac{\Delta H^{\text{F}}_{\text{NaCl}}}{RT}\left(\frac{T}{T^{\text{F}}_{\text{NaCl}}} - 1\right) - \frac{v_{\text{NaCl}}}{RT}(\delta_{\text{water}} - \delta_{\text{NaCl}})^2 - 1 + \frac{v_{\text{NaCl}}}{v_{\text{water}}} - \ln\left(\frac{v_{\text{NaCl}}}{v_{\text{water}}}\right) \tag{13}$$

where $\Delta H^{\text{F}}_{\text{NaCl}}$ and $T^{\text{F}}_{\text{NaCl}}$ stand, respectively for the heat of fusion (J mol^{-1}) and the melting point of NaCl (K), while v_k and δ_k represent the molar volume (m^3 mol^{-1}) and the solubility parameter of the species k ((J m^{-3})$^{1/2}$).

The solubility parameter for water is calculated using the expression proposed by Sagara et al. [21]:

$$\delta_{\text{water}} = \frac{(6v^{\text{solid}}_{\text{water}}\varepsilon N^0)^{0.5}}{v_{\text{water}}} \tag{14}$$

where $v^{\text{solid}}_{\text{water}}$ stands for the solid molar volume of water. The value proposed by Wagner and Kruse [22] was used in this study. N^0 is Avogadro's number (mol^{-1}) and ε is the pair potential energy (J). These values are computed according to Higashi et al. [23]. Finally, the molar volume of water vapour, v_{water}, is computed following the relations established in IAPWS-IF97 [16]:

The solubility parameter of NaCl is given by [24]:

$$\delta_{\text{NaCl}} = \left(\frac{\Delta u_{\text{NaCl}}}{v_{\text{NaCl}}}\right)^{0.5} \tag{15}$$

where Δu_{NaCl} is the cohesive energy of NaCl. The dependence upon the temperature of this energy is computed according to Higashi et al. [23]:

$$\Delta u_{\text{NaCl}} = 0.16491T + 14.23 \tag{16}$$

v_{NaCl} is the molar volume of NaCl. It is calculated following the work proposed by Iwai et al. [25]:

$$\ln(v_{\text{NaCl}}) = \alpha^v_{\text{NaCl}} \ln(\rho_{\text{water}}) + \beta^v_{\text{NaCl}} \tag{17}$$

The parameters α^v_{NaCl} and β^v_{NaCl} are dimensionless parameters estimated by Shin et al. [20].

All the parameters used for calculate the solubility of NaCl in the vapour phase are accessible Table 1.

Table 1
Parameters used to compute the solubility of NaCl in the vapour phase according to Shin et al. [15]

Parameter	Value	Reference
$\Delta H^{\text{F}}_{\text{NaCl}}$ (J mol^{-1})	28200	[26]
$T^{\text{F}}_{\text{NaCl}}$ (K)	1074	[26]
$v^{\text{solid}}_{\text{water}}$ (m^3 mol^{-1})	1.963×10^{-5}	[17]
ε	9.3926×10^{-21}	[18]
α^v_{NaCl}	-1	[15]
β^v_{NaCl}	-2.62	[15]

During the expansion, some liquid water might be formed in the capillary. Because of the higher solubility of NaCl in this phase than in the vapour one, specific attention must be paid to this phase. Indeed the following equilibrium has to be taken into account:

$$\text{NaCl}_{\text{sol}} \leftrightarrow \text{Na}_{\text{acq}}{}^{+} + \text{Cl}_{\text{acq}}{}^{-} \tag{18}$$

To describe pure salt solubility in the aqueous phase, we use the mathematical form of the liquid solid equilibrium:

$$\prod_i \left(\frac{m_i}{m^0}\gamma_i\right)^{\nu_i} - K(T) = 0 \tag{19}$$

where m_i is the molality of species i and m^0 is the unit molality. In the preceding expression, γ_i stands for the activity coefficient of the species under inspection while ν_i represents its stoichiometric coefficient in the equilibrium relation. Finally, the equilibrium constant K is computed from the definition of the standard Gibbs free energy:

$$\ln(K) = -\frac{\Delta G^{\circ}_{\text{R}}}{RT} \tag{20}$$

This energy was computed using the standard molal Gibbs' free energy taken from the SUPCRT92 computer program data file [26].

Pitzer's model [27] was used in order to evaluate the activity coefficients. There are numerous articles, which give complete details of the Pitzer equations. For an electrolyte CA with ν_C cation of charge z_C and ν_A anion of charge z_A, the mean activity coefficient is given by

$$\ln(\gamma_{CA}^{\pm}) = -|z_C z_A| A^{\phi} \left[\frac{I^{1/2}}{1 + bI^{1/2}} + \frac{2}{b} \ln(1 + bI^{1/2}) \right] + m \frac{2\nu_C \nu_A}{\nu_C + \nu_A} B_{CA}^{\gamma} + m^2 \frac{2(\nu_C \nu_A)^{3/2}}{\nu_C + \nu_A} C_{CA}^{\gamma} \quad (21)$$

where b is an empirical parameter fixed at 1.2, m the mean molality the electrolyte CA, I the ionic strength and A^{ϕ} is the Debye–Hückel parameter expressed in specific units [28]:

$$A^{\phi} = \frac{1}{3} \left(\frac{2\pi N^0 \rho_w^{A^{\phi}}}{1000} \right)^{1/2} \left(\frac{(e^{esu})^2}{\psi k_B^{erg} T} \right)^{3/2} \quad (22)$$

In Eq. (22), $\rho_w^{A^{\phi}}$ is the density of aqueous solution ($g\,cm^{-3}$), k_B^{erg} the Boltzmann's constant in erg (1.38045×10^{-16} erg), T the absolute temperature (K), ψ the water dielectric constant and e^{esu} is the electronic charge in esu (4.8029×10^{-10} esu).

In Eq. (21), C_{CA}^{γ} and B_{CA}^{γ} are parameters of the model and they are computed according to:

$$C_{CA}^{\gamma} = \frac{3}{2} C_{CA}^{\phi}, \quad (23)$$

$$B_{CA}^{\gamma} = B_{CA} + B_{CA}^{\phi} \quad (24)$$

where

$$B_{CA}^{\phi} = \beta_{CA}^{(0)} + \beta_{CA}^{(1)} \exp(-\alpha_1 I^{1/2}) + \beta_{CA}^{(2)} \exp(-\alpha_2 I^{1/2}) \quad (25)$$

and

$$B_{CA} = \beta_{CA}^{(0)} + \beta_{CA}^{(1)} g(\alpha_1 I^{1/2}) + \beta_{CA}^{(2)} g(\alpha_2 I^{1/2}) \quad (26)$$

where the function g is defined as:

$$g(x) = \frac{2}{x^2} [1 - (1 + x) \exp(-x)] \quad (27)$$

For a salt with at least one univalent cation or anion like NaCl, $\alpha_1 = 2$ and $\beta_{CA}^{(2)} = 0$ [28,29]. $\beta_{CA}^{(0)}$, $\beta_{CA}^{(1)}$ and C_{CA}^{ϕ} are electrolyte specific parameters functions of the temperature and the pressure. We use the function proposed by Pitzer et al. [30]:

$$f(T, P) = \frac{q_1}{T} + q_2 + q_3 P + q_4 P^2 + q_5 P^3 + q_6 \ln(T) + (q_7 + q_8 P + q_9 P^2 + q_{10} P^3) T + (q_{11} + q_{12} P + q_{13} P^2) T^2 + \frac{(q_{14} + q_{15} P + q_{16} P^2 + q_{17} P^3)}{T - 227} + \frac{(q_{18} + q_{19} P + q_{20} P^2 + q_{21} P^3)}{680 - T} \quad (28)$$

The parameters necessary for $NaCl/H_2O$ system are given in Table 2.

The preceding equations yield the respective solubility of NaCl in the vapour and the liquid phases. The model is completed using mass balances that compute the distribution of the salt between each phase.

Table 2
$\beta_{CA}^{(0)}$, $\beta_{CA}^{(1)}$, C_{CA}^{ϕ} parameters for the H_2O/NaCl system ($-273 < T < 573$ K and $-1 < P < 1000$ bar)

Parameters	$\beta_{CA}^{(0)}$	$\beta_{CA}^{(1)}$	C_{CA}^{ϕ}
Q_1	−656.81518	119.31966	−6.1084589
Q_2	24.8691295	−0.48309327	4.0217793×10^{-1}
Q_3	$5.381275267 \times 10^{-5}$	0.0	2.2902837×10^{-5}
Q_4	$-5.58874699 \times 10^{-8}$	0.0	0.0
Q_5	$6.58932633 \times 10^{-12}$	0.0	0.0
Q_6	−4.4640952	0.0	−0.075354649
Q_7	0.01110991383	1.4068095×10^{-3}	$1.531767295 \times 10^{-4}$
Q_8	$-2.657339906 \times 10^{-7}$	0.0	$-9.0550901 \times 10^{-8}$
Q_9	$1.746006963 \times 10^{-10}$	0.0	0.0
Q_{10}	$1.0462619 \times 10^{-14}$	0.0	0.0
Q_{11}	$-5.307012889 \times 10^{-6}$	0.0	$-1.53860082 \times 10^{-8}$
Q_{12}	$8.634023325 \times 10^{-10}$	0.0	$8.6926600 \times 10^{-11}$
Q_{13}	$-4.1785962 \times 10^{-13}$	0.0	0.0
Q_{14}	−1.579365943	−4.2345814	0.3531041306
Q_{15}	$2.202282079 \times 10^{-3}$	0.0	$-4.33144252 \times 10^{-4}$
Q_{16}	$-1.310550324 \times 10^{-7}$	0.0	0.0
Q_{17}	$-6.3813688333 \times 10^{-11}$	0.0	0.0
Q_{18}	9.706578079	0.0	−0.09187145529
Q_{19}	−0.02686039622	0.0	5.1904777×10^{-4}
Q_{20}	$1.534474401 \times 10^{-5}$	0.0	0.0
Q_{21}	$-3.215398267 \times 10^{-9}$	0.0	0.0

Table 3
Influence of the capillary diameter on the total length of the device and on the salt distribution at the exhaust

Diameter of the capillary, d ($\times 10^{-3}$ m)	Total length of the capillary, L (m)	Occurrence of the liquid phase, L_{sat} (m)	Percentage of NaCl in the solid phase, %Sol	Percentage of NaCl in the vapour phase, %Vap	Percentage of NaCl in the liquid phase, %Liq
0.8	0.624	0.610	85.28	0.00	14.72
1.6	21.515	21.486	96.58	0.00	3.42
3.2	608.330	608.241	99.23	0.00	0.77
6.4	16670.618	No occurence	100.00	0.00	0.00

4. Results

4.1. Diameter of the capillary

As it has been quoted in the introduction, the model is firstly used to check the influence of the diameter of the capillary on its length and also on the distribution of NaCl at the output. Table 3 sums us these results. It can be observed that the higher the diameter is, the longer the capillary device must be. Indeed, for small diameter devices, friction forces are much more important leading to a smaller length. For example the length of the 6.4 mm capillary device is approximately 17 km whereas it is only 0.624 m for a 0.8 mm device. Thus one could conclude that the smallest internal diameter is the better. However, the percentage of NaCl dissolved in the liquid phase decreases when the internal diameter increases. Fig. 2 gives an explanation about this phenomenon. This figure illustrates the two expansions in the (P–T) diagram. What can be seen in that diagram is that for lower diameters the expansion pathway is such that the saturation curve is reached quicker than for higher diameters. The reason for this quicker appearance of liquid state is that the shorter the diameter is, the higher the speed of the fluid is. These higher speeds lead to higher pressure drop and because of mechanical energy conservation, to a more important decrease in the temperature of the stream at a given pressure. This leads to value of the vapour fraction of $\omega = 0.988$ and 0.997 for the respective diameters of 0.8 and 1.6 mm. This lower value of the vapour fraction means that more liquid water has been formed at the end of the device. Because the solubility of NaCl is higher in the liquid phase than in the vapour one, the final amount of salt in the liquid phase is higher. Thus two opposite conclusions might be drawn regarding the length of the device or the distribution of salt at the output. Because of its lower size, we have finally chosen to focus our studies on the 1.6 mm diameter device.

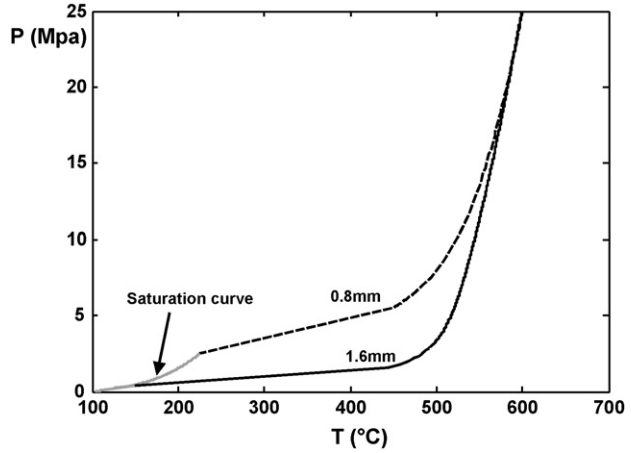

Fig. 2. P–T diagram of the expansion for capillary diameters of 0.8 and 1.6 mm.

4.2. Expansion at nominal conditions

Figs. 3–5 show the evolution of the state variables of the system a s a function of the distance from the inlet of the device for an adiabatic expansion operated at nominal conditions ($\dot{m}_{in} = 20\,kg\,h^{-1}$, $P_{in} = 25$ MPa, $T_{in} = 873$ K, $C_{in} = 0.5\,mol\,l^{-1}$). Figs. 3 and 4 should be studied together because there is a high

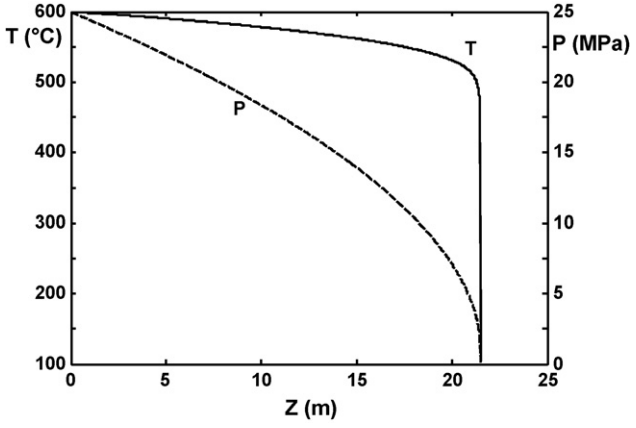

Fig. 3. Evolution of temperature and pressure as a function of position inside the capillary device for nominal expansion.

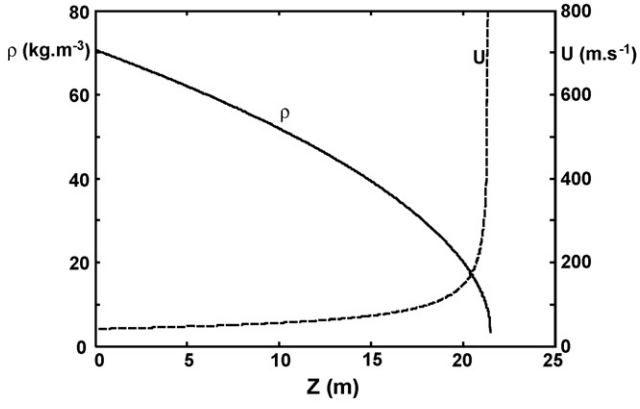

Fig. 4. Evolution of density and velocity as a function of position inside the capillary device for nominal expansion.

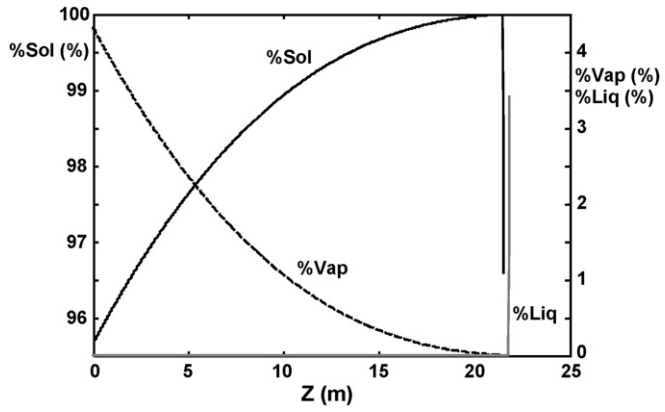

Fig. 5. Evolution of ratio of NaCl held in the solid phase, the liquid phase and the vapour phase as a function of position inside the capillary device for nominal expansion.

coupling between the variables P, T, ρ and U. Indeed, the pressure drop firstly leads to a decrease in the density of the fluid. For total mass conservation this density decrease leads to an increase in the velocity of the fluid, what in turns (because of total energy conservation) induces a lowering of the temperature. By the end of the capillary, the density becomes so small that the velocity becomes very high and creates very high temperature gradient at this position. These phenomena have to be taken into account for future design of the device. Fig. 5 represents the distribution of NaCl in the different phases as a function of position in the device. The curve representing the liquid fraction has voluntary be translated to the right in order see both the stiff decrease in the solid phase and increase in the liquid phase. This stiff behaviour is linked to the occurrence of liquid water at this position: once liquid water appears, out equilibrium calculation saturates the liquid fraction into NaCl up to its solubility at this point.

4.3. Influence of the operating conditions

Table 4 summarises the influence of the inlet temperature on the properties of the expanded flow. The main influence of this parameter is relative to the inlet velocity of the fluid. If the temperature is rose, the inlet density is also decreased what increases the inlet velocity of the fluid. Finally, this leads to a decrease in the total length of the capillary. However, one can notice that the temperature does not exercise a great influence on the salt distribution at the output.

Table 5 shows the influence of the initial mass flow rate of incoming water on the properties of the output of the device. Once again, the impact of the total mass flow rate is linked to the initial velocity of the fluid. For a given set of inlet pressure and temperature, an increase in the total mass flow rate leads to an increase in the inlet velocity. Finally, one can observe that the higher the mass flow rate is, the shorter the length is. As it was explained in the paragraph devoted to the description of the diameter, longer expansion leads however to a smaller amount of salt in the liquid phase, the occurrence of the liquid phase being translated towards the output of the device.

Table 6 shows the influence of the external heat transfer coefficient. From adiabatic to free convection with the surroundings ($H \approx 30\,\mathrm{W\,m^{-2}\,K^{-1}}$), there is no significant evolution of the output data. This means that the heat losses to the surroundings do not contribute significantly to Eq. (7). This also means that there is no need to perfectly insulate the device.

To conclude with the influence of the operating parameters, Fig. 6 gives the influence of the initial salt composition on its final distribution between the liquid phase and the vapour phase. Because the computation of solubilities is post processed from the results of the expansion calculation, the initial concentration of salt does not have any influence on the evolution of these solubilities inside the tube. It is just that for very low inlet con-

Table 4
Influence of the inlet temperature on the total length of the device and on the salt distribution at the exhaust

Inlet temperature, T_{in} (°C)	Total length of the capillary, L (m)	Occurrence of the liquid phase, L_{sat} (m)	Percentage of NaCl in the solid phase, %Sol	Percentage of NaCl in the vapour phase, %Vap	Percentage of NaCl in the liquid phase, %Liq
700	17.782	17.760	96.88	0.00	3.12
650	19.434	19.409	96.76	0.00	3.24
600	21.515	21.486	96.58	0.00	3.42
550	24.278	24.245	96.29	0.00	3.71
500	28.382	28.240	95.96	0.00	4.04
400	35.164	35.092	95.24	0.00	4.76

Table 5
Influence of the inlet mass flow rate on the total length of the device and on the salt distribution at the exhaust

Inlet mass flow rate, $\dot{m}_{in}$ (kg h^{-1})	Total length of the capillary, L (m)	Occurrence of the liquid phase, L_{sat} (m)	Percentage of NaCl in the solid phase, %Sol	Percentage of NaCl in the vapour phase, %Vap	Percentage of NaCl in the liquid phase, %Liq
30	10.123	10.095	94.83	0.00	5.17
25	14.241	14.213	95.62	0.00	4.38
20	21.515	21.486	96.58	0.00	3.42
15	36.390	36.360	97.45	0.00	2.55
10	75.656	75.624	98.70	0.00	1.30
5	259.985	259.947	99.33	0.00	0.67

Table 6
Influence of the heat transfer coefficient on the total length of the device and on the salt distribution at the exhaust

Heat transfer coefficient, H ($W\,m^{-2}\,K^{-1}$)	Total length of the capillary, L (m)	Occurrence of the liquid phase, L_{sat} (m)	Percentage of NaCl in the solid phase, %Sol	Percentage of NaCl in the vapour phase, %Vap	Percentage of NaCl in the liquid phase, %Liq
0	21.515	21.486	96.58	0.00	3.42
5	21.183	21.152	96.63	0.00	3.37
10	20.851	20.824	96.66	0.00	3.34
15	20.537	20.501	96.74	0.00	3.26
20	20.215	20.190	96.75	0.00	3.25
25	19.916	19.895	96.82	0.00	3.18
30	19.614	19.590	96.82	0.00	3.18

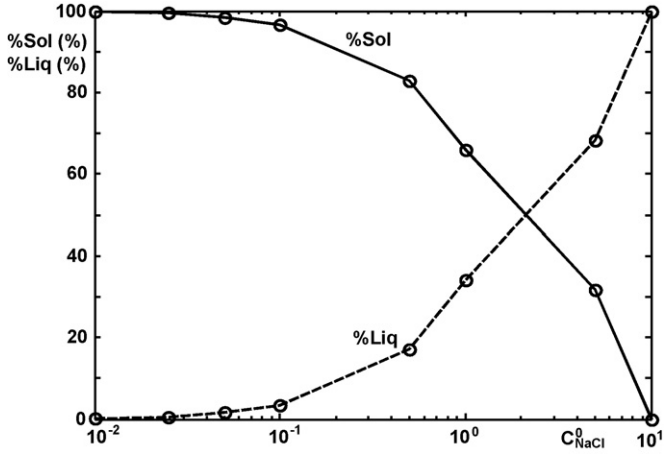

Fig. 6. Influence of the initial concentration of NaCl on the ratio of NaCl held in the solid phase, the liquid phase and the vapour phase at the output of the capillary device.

centration, the final solubility of salt in the liquid phase is higher than its initial concentration in the mixture. The whole amount of the incoming salt is dissolved in liquid water at the exhaust of the device. Intermediate results can be observed for the whole range of incoming salt concentrations.

5. Conclusion

This paper deals with theoretical expansion of supercritical water, loaded with salts, into a capillary device. A mathematical model for the flow field has been developed. Basically, it is based on the mass balance equation, the momentum equation and the energy conservation equation. It is completed with the assumption of pure water behaviour for the computation of the density of the media as well as for its enthalpy to weight. From the prediction of salt distribution point of view, a thermodynamic approach has been used. It allows for the computation of the solubilities of NaCl within the liquid and the vapour phase, leading in turns (with the aim of a mass balance) to the amount of salt present in each phase.

Using this model it has been possible to enhance our knowledge of how such an expansion is processed within a capillary device. Details have been given on how the pressure drop, linked to the friction of the flow with the capillary material, exercises modifications of the value of the fluid density and in turns on its temperature. It has also shown the importance of the thermal gradients and velocities near the output of the tube. Such considerations have to be carefully taken into account for future design of the apparatus. However, the model has also helped us to make our choice for the diameter of the device. A value of 1.6 mm seems to correspond to our specifications (in terms of total length of the device and amount of dissolved salt). Moreover the model enhances our confidence in terms of possibility of separation of the salts from the flow. Our computations have shown that a maximum value of 5.17% of the incoming salt (if sufficiently concentrated) might be dissolved into liquid water. We would like to point out that this is a thermodynamical computation, what means that this represents the maximal value that might be observed. However, because of the high value speed of the flow near the output of the device, we expect that the residence time of the fluid inside the tube once liquid has appeared will not be sufficient for dissolution to effectively occur. This would mean that qt the output of the device it is possible to separate the solid from the exhausting fluid at atmospheric condition.

Acknowledgments

We wish to thank the French minister of economy and the European Union (Interreg IIIb, Atlantic area) for their financial support to this work in the Frame of the SUPERMAT network.

References

[1] P. Dutournié, Modélisation de réacteurs d'oxydation de déchets organiques en milieu aqueux supercritique, PhD Thesis, Université de Pau et des Pays de l'Adour, 2000.
[2] F. Cansell, S. Rey, P. Beslin, Thermodynamic aspect of supercritical fluids processing: applications to polymers and wastes treatment, Revue de l'Institut Français du Pétrole 53 (1998) 71–98.
[3] F. Cansell, P. Beslin, B. Berdeu, Hydrothermal oxidation of model molecules and industrial wastes, Environ. Prog. 17 (1998) 240–245.
[4] J.W. Tester, H.R. Holgate, F.J. Amellini, P.A. Webley, W.R. Killilea, G.T. Hong, H.E. Barner, Supercritical water oxidation technology. Process development and fundamental research, ACS Symp. Ser. 518 (1993) 35–76.
[5] K.A. Smith, J.G. Harris, J.B. Howard, J.W. Tester, P. Griffith, H.J. Herzog, W.A. Peters, R.M. Latanision, Supercritical water oxidation: principles and prospects, in: Official Proceedings of the 56th International Water Conference, 1995, pp. 468–478 [S.1]: [s.n].
[6] M. Hodes, P.A. Marrone, G.T. Hong, K.A. Smith, J.W. Tester, Salt precipitation and scale control in supercritical water oxidation. Part A. Fundamentals and research, J. Supercrit. Fluid 29 (2004) 265–288.

[7] V.M. Valyashko, Phase equilibria in water–salt systems: some problems of solubility at elevated temperature and pressure, in: R.W. Staehle, D.G. Jones, J.E. Slater, I. Tome (Eds.), High Temperature High Pressure Electrochemistry in Aqueous Solutions, 1973, pp. 153–157.
[8] M. Hodes, P.A. Marrone, G.T. Hong, K.A. Smith, J.W. Tester, Salt precipitation and scale control in supercritical water oxidation. Part A. Fundamentals and research, J. Supercrit. Fluid 29 (2004) 265–288.
[9] M. Hodes, P.A. Marrone, G.T. Hong, K.A. Smith, J.W. Tester, Salt precipitation and scale control in supercritical water oxidation. Part B. Commercial/full-scale applications, J. Supercrit. Fluid 29 (2004) 289–312.
[10] L. Ott, V. Lehr, S. Urfels, M. Bicker, H. Vogel, Influence of salts on the dehydration of several biomass-derived polyols in sub- and supercritical water, J. Supercrit. Fluid 38 (2006) 80–93.
[11] M.D. Bermejo, A. Martin, J.L. Florusse, C.J. Peters, M.J.V.M. Cocero, Bubble points of the systems isopropanol–water, isopropanol–water–sodium acetate and isopropanol–water–sodium oleate at high pressure, Fluid Phase Equilib. 244 (2006) 78–85.
[12] M.D. Bermejo, A. Martin, J.L. Florusse, C.J. Peters, M.J. Cocero, The influence of Na_2SO_4 on the CO_2 solubility in water at high pressure, Fluid Phase Equilib. 238 (2005) 220–228.
[13] C.S. Laspidou, D.F. Lawler, E.F. Gloyna, B.E. Rittmann, Heather effects on cyclone performance for the separation of solids from high temperature and pressure effluents, Sep. Sci. Technol. 34 (15) (1999) 3059–3076.
[14] P.C. Dell'Orco, L. Li, E.F. Gloyna, The separation of particulates from supercritical water oxidation processes, Sep. Sci. Technol. 28 (1–3) (1993) 625–642.
[15] W.R. Killilea, G.T. Hong, K.C. Swallow, T.B. Thomason, Supercritical water oxidation: microgravity solids separation, SAE Technical Paper Series, No. 881038, 1988.
[16] W. Wagner, A. Kruse, The industrial standard IAPWS-IF97 for the thermodynamic properties and supplementary equations for other properties, in: Properties of Water and Steam, Springer, 1998.
[17] D. Kodra, V. Balakotaiah, Modeling of oxidation of aqueous waste in a deep well reactor, AIChE J. 38 (7) (1992) 988–1002.
[18] I.E. Idel'cik, Memento des Pertes de Charge, Editions Eyrolles, 1986.
[19] P. Chassaing, in: Cepaduès (Ed.), Mécanique des fluides—Eléments d'un premier cours, collection Polytech.
[20] H.Y. Shin, K. Matsumoto, H. Higashi, Y. Iwai, Y. Arai, Development of a solution model to correlate solubilities of inorganic compounds in water vapor under high temperatures and pressures, J. Supercrit. Fluid 21 (2001) 105–110.
[21] H. Sagara, Y. Arai, S. Saito, Calculation of Henry's constant of gases in hydrocarbon solvent by regular solution theory, J. Chem. Eng. Jpn. 8 (1975) 93–97.
[22] W. Wagner, A. Kruse, Properties of Water and Steam, Springer, Tokyo, Japan, 1998.
[23] H. Higashi, Y. Iwai, K. Matsumoto, Y. Kitani, F. Okazaki, Y. Shimoyama, Y. Arai, Measurement and correlation for solubilities of alkali metal chlorides in water vapor at high temperature and pressure, Fluid Phase Equilib. (2004).
[24] A.F.M. Barton, Handbook of Solubility Parameters and Other Cohesion Parameters, CRC Press, Boca Raton, FL, 1983.
[25] Y. Iwai, Y. Koga, T. Fukuda, Y. Arai, Correlation of solubilities of high-boiling components in supercritical carbon dioxide using a solution model, J. Chem. Eng. Jpn. 25 (1992) 757–760.
[26] J.W. Johnson, E.H. Oelkers, H.C. Helgelson, SUPCRT92: a software package for calculating the standard molal thermodynamic properties of minerals, gases, aqueous species reactions from 1 to 5000 bar and 0–1000 °C, Comput. Geosci. 18 (1992) 899–947.
[27] K.S. Pitzer (Ed.), Activity Coefficients in Electrolyte Solutions, 2nd ed., CRC Press, Boca Raton, FL, 1991, pp. 75–153.
[28] J.F. Zemaitis, D.M. Clark, M. Rafal, N.C. Scrivner, Handbook of Aqueous Electrolyte Thermodynamics, DIPPR, AIChE, New York, 1986.
[29] H. Carrier, S. Ye, I. Vanderbrecken, J. Li, P. Xans, Salt solubility under high pressure and high temperature, High Temp. High Press. 30 (1998) 629–634.
[30] K.S. Pitzer, J.C. Peiper, R.H. Busey, Thermodynamic properties of aqueous sodium chloride solutions, J. Phys. Chem. Ref. Data 13 (1) (1984) 1–102.